

NUMERICAL SIMULATION OF ACTIVE CONTROL OF TRANSONIC FLUTTER

L. Djayapertapa & C. B. Allen
Department of Aerospace Engineering,
University of Bristol, Bristol, BS8 1TR, U.K.
L. Djayapertapa now at Airbus UK,
Aerodynamics Design & Data,
Airbus UK, Building 7DO,
Filton, Bristol, BS99 7AR.

Email: C.B.Allen@Bristol.ac.uk Lesmana.Djayapertapa@airbus.com

Keywords: *Unsteady flow, Euler equations, Moving meshes, Aeroelastic coupling, Active control*

Abstract

Independent structural dynamic and inviscid aerodynamic models are coupled, in the time domain, and two-dimensional transonic flutter suppression via active flap control is simulated. The two common coupling approaches, namely ‘weak’ and ‘strong’ procedures, are investigated and it is found that the strong coupling scheme is more accurate than the weak coupling approach, and only for large real time-steps is the strong coupling scheme more expensive. The method developed is used to simulate transonic aeroelasticity in the time domain, and to compute stability (flutter) boundaries of 2-D wing sections. A control law is then implemented within the solver to investigate active control of a trailing edge flap. Open and closed loop simulations show that active control can successfully suppress flutter and results in a significant increase in the allowable speed index in the transonic regime.

1 Introduction

In the transonic region the structural loads, and hence aeroelastic behaviour, are greatly affected

by the presence and motion of shock waves. Hence, the accurate prediction of flutter characteristics of aerofoils in transonic flow is a critical design consideration for most modern civil and high performance aircraft.

In the pure subsonic or supersonic regimes it has been normal industry practice to use linear aerodynamic theory, such that the aerodynamic forces depend upon the body motion in linear fashion, thus permitting uncoupling of the structural and fluid equations [1]. However, this can not be applied in the transonic regime due to the high non-linearity of the flow field. There are other nonlinear phenomena associated with aeroelastics, for example aileron buzz or limit cycle oscillations (LCO), and none of these phenomena can be predicted directly by traditional linear theoretical methods, since they are interactions between nonlinear aerodynamic forces and structures. Hence, more advanced aeroelastic simulation methods, applicable to transonic flows, are essential.

Coupling independent aerodynamic (CFD) and structural dynamics (CSD) codes in the time domain allows time-accurate simulation of aeroelastic response, and the possibility of identifying flutter boundaries. (Adding a flight control system allows aeroservoelastic simulation.) It is possible, with current computational power,

Copyright©2002 by C.B. Allen. Published by the International Council of the Aeronautical Sciences, with permission

to develop such coupled methods using the Euler and Navier-Stokes equations as the aerodynamic model. Euler solvers have been coupled with structural models previously, see for example [2]-[7]. The Navier-Stokes equations are still rarely used in computational transonic aeroelasticity due mainly to their excessive CPU demands. Simplified forms of the Navier-Stokes equations have been used for aeroelastic applications, see for example [8] - [12], but results show that for two degree of freedom aerofoil motions little difference was found between using inviscid and viscous aerodynamic models.

The time-accurate interaction between structural dynamics, the flight control system and aerodynamics, known as aeroservoelasticity, has recently received attention, see for example [15]-[26]. Active Control Technology (ACT) can be implemented within an aeroelastic solver in order to simulate any the following: flutter suppression, gust alleviation or manoeuvre enhancement. Previous work has relied mainly on transonic small disturbance theory as the aerodynamic solver [21, 22, 23], or has been performed in the frequency domain [19] - [27]. For example, Nissim [19, 27] performed flutter boundary calculations in the frequency domain by considering the sign of the work done by the structural system on its surroundings. There are limitations to this approach, but the energy analysis is extremely useful and is used here.

Conventional active control systems have constant (with time) control laws. However, the use of adaptive control in active flutter suppression has started to appear in the literature, see for example [24, 25, 26]. This approach is attractive since the parameters of the system often change with time or under load, which is the usual limitations of control using fixed-structures, fixed-parameter controllers. The added complexity of adaptive control is often justified by reduced hardware requirements, but it is very difficult to prove the stability properties of controllers whose parameters can vary. In addition, it is almost impossible to get certification for civil aircraft equipped with adaptive control. Hence, the approach of using fixed-parameter controllers is

preferred in this research, although it should also be noted that fixed-parameter active controllers are also difficult to certify.

This paper presents a computational method to simulate aeroelastic and aeroservoelastic behaviour of a two and three degree of freedom aerofoil. The aerodynamic model is described by the Euler equations, which is coupled with a structural model, and the two common coupling approaches, namely weak and strong time-domain coupling, are considered. A control law is implemented within the aeroelastic solver to investigate active means of flutter suppression via control surface (flap) motion, and the effect on the stability (flutter) boundary presented. The mechanics of flutter are examined by considering the phase difference between heave and pitch motions for a two degree-of-freedom model.

2 Structural Model

Figure 1 shows the typical three degree of freedom wing section used to derive the structural equations of motion. This model has been well established for two dimensional aeroelastic analysis [39]. The pitching and heaving displacements are restrained by a pair of spring attached to the elastic axis (EA) with spring constants K_α and K_h respectively. A torsional spring is also attached at the hinge axis whose spring constant is K_β .

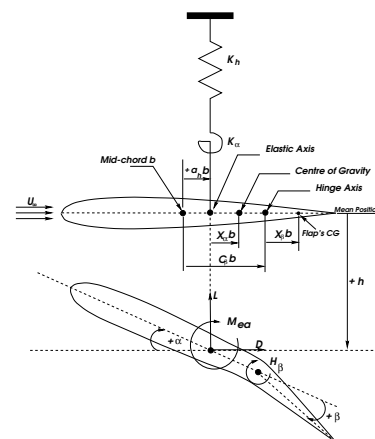


Fig. 1 Aeroelastic parameter definition.

The governing equations of motion for the three degree of freedom system are given by :

$$m\dot{h} + S_\alpha b\ddot{\alpha} + S_\beta b\ddot{\beta} + K_h h = -L \quad (1)$$

$$S_\alpha b\ddot{h} + I_\alpha \ddot{\alpha} + [(C_\beta - a_h) b S_\beta + I_\beta] \ddot{\beta} + K_\alpha \alpha = M_{ea} \quad (2)$$

$$S_\beta \dot{h} + [(C_\beta - a_h) b S_\beta + I_\beta] \ddot{\alpha} + I_\beta \ddot{\beta} + K_\beta \beta = H_\beta \quad (3)$$

where the symbol definitions are given in figure 1. S_α is the static moment of the aerofoil about the elastic axis and is given by $S_\alpha = mX_\alpha b$. S_β is the static moment of the control surface about the hinge axis and is given by $S_\beta = mX_\beta b$. $I_\alpha = mr_\alpha^2 b^2$ is the aerofoil moment of inertia about the elastic axis, and $I_\beta = mr_\beta^2 b^2$ is the control surface moment of inertia about the elastic axis.

In order to get the full non-dimensional form of the equation, non dimensional heave ($\xi = \frac{h}{b}$) and non dimensional time is introduced. The full non-dimensional form of the aeroelastic equations can be written in the form

$$[M]\mathbf{q}'' + [K]\mathbf{q} = \mathbf{f}_a \quad (4)$$

where

$$[M] = \begin{bmatrix} 1 & x_\alpha & x_\beta \\ x_\alpha & r_\alpha^2 & (C_\beta - a_h)x_\beta + r_\beta^2 \\ x_\beta & (C_\beta - a_h)x_\beta + r_\beta^2 & r_\beta^2 \end{bmatrix} \quad (5)$$

$$[K] = \frac{4M_\infty^2 \gamma}{U^{*2} \mu} \begin{bmatrix} \frac{\omega_h^2}{\omega_\alpha^2} & 0 & 0 \\ 0 & r_\alpha^2 & 0 \\ 0 & 0 & r_\beta^2 \frac{\omega_\beta^2}{\omega_\alpha^2} \end{bmatrix}, \quad (6)$$

$$\mathbf{q} = \begin{Bmatrix} \xi \\ \alpha \\ \beta \end{Bmatrix}, \quad \mathbf{f}_a = \frac{4M_\infty^2 \gamma}{\pi \mu} \begin{Bmatrix} -C_L \\ 2C_{M_{ea}} \\ 2C_H \end{Bmatrix} \quad (7)$$

U^* and μ are the non-dimensional speed (the speed index) and mass ratio of aerofoil to air respectively, and their expressions are given by

$$U^* = \frac{U_\infty}{b \omega_\alpha \sqrt{\mu}} ; \quad \mu = \frac{m}{\pi \rho b^2} \quad (8)$$

Equation 4 is solved by approximating it at time level $n + 1$, and an implicit Newmark scheme [40] is used to integrate the equation.

3 Aerodynamic Model

A finite-volume Euler code is used for the aerodynamic model. The two-dimensional unsteady Euler equations on a moving grid in integral form are :

$$\frac{\partial}{\partial t} \iint_A \mathbf{U} dx dy + \int_{\partial A} \mathbf{F} \cdot \mathbf{n} dS = 0 \quad (9)$$

where \mathbf{U} is the vector of conserved variables, \mathbf{F} is the flux vector, \mathbf{n} is the outward cell face unit normal, and S the peripheral length of the cell face. \mathbf{U} and \mathbf{F} are given by:

$$\mathbf{U} = \begin{Bmatrix} \rho \\ \rho u \\ \rho v \\ \rho e \end{Bmatrix}, \quad \mathbf{F} = \begin{Bmatrix} \rho(\mathbf{u} - \mathbf{X}_t) \\ \rho u(\mathbf{u} - \mathbf{X}_t) + P\mathbf{i} \\ \rho v(\mathbf{u} - \mathbf{X}_t) + P\mathbf{j} \\ \rho e(\mathbf{u} - \mathbf{X}_t) + P\mathbf{u} \end{Bmatrix} \quad (10)$$

where \mathbf{u} is the velocity vector, \mathbf{X}_t the grid velocity vector, and P , ρ , u , v and e are pressure, density, Cartesian x- and y-component velocities and total specific energy respectively. The equation set is closed by

$$P = (\gamma - 1) \left(\rho e - \frac{\rho \mathbf{u}^2}{2} \right) \quad (11)$$

3.1 Discretisation

The unsteady Euler equations are solved using a Jameson [28] type cell-centred finite-volume method. Equation 9 is applied to each cell of the mesh. Following Jameson *et al* [28], the spatial and time dependent terms are decoupled and a set of ordinary differential equations is obtained. Artificial dissipation needs to be added to stabilise the solution [28, 29].

An efficient implicit time-integration scheme is used, based on that proposed by Jameson [30]. This solves unsteady flows as a series of pseudo-steady cases, and is extremely efficient compared to an explicit scheme [31, 36]

3.2 Moving Mesh Algorithm

The flow-solver is used in conjunction with a structured moving mesh, which allows the cell

volumes to distort as the aerofoil moves or deforms. An algebraic moving grid generator based on transfinite interpolation [32] - [34] is used. This approach is extremely efficient, as it allows instantaneous grid positions and speeds to be computed directly at any time [35, 36].

In order to avoid conservation errors a geometric conservation law for the cell volumes needs to be satisfied numerically, in addition to the conservation laws that governs the physics of the flow [37]. More details of the flow-solver can be found in [38].

4 Coupling Approach

The simplest method to couple separate aerodynamic and structural dynamic codes is ‘weak’ coupling, wherein there is no intermediate exchange of information between the two solvers at each time level. At each time level the fluid is solved using the current structural position to give aerodynamic loads on the structure, and these are then used to solve for a new structural position. This is simply repeated for each time level. Hence, the fluid and structure are not synchronised in time, and there is always a phase lag between the two. This phase lag will be time-step dependent, and this is considered later.

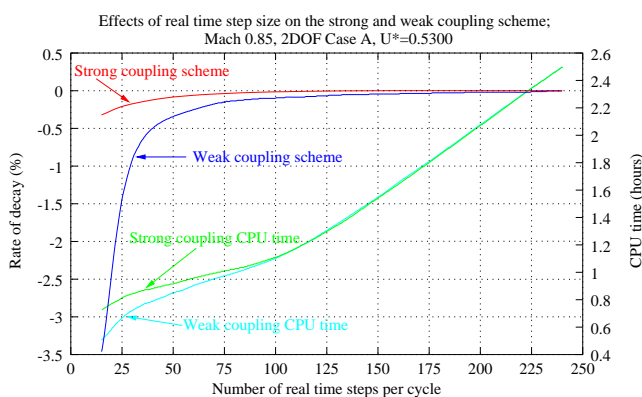


Fig. 2 Weak and strong coupling schemes.

Alternatively ‘strong’ coupling can be used, wherein there is exchange of information between the two solvers. At each real time level the aerodynamic loads are computed, then the structural position that result from those loads computed. The aerodynamic loads around this new

structural position are then recomputed, and this iterative procedure is repeated until the fluid and structure are perfectly synchronised at each real time level. A flight control system is integrated with the aero-structural code in the next section, and it is clearly desirable that no phase lag is present in this case.

4.1 Method Comparison

For coupled calculations, first a converged steady flow solution about the aerofoil was computed. The aerofoil was then given a disturbance in the form of vertical velocity (and pitch rate), and the subsequent response of the system obtained by simultaneously integrating the structural and the aerodynamic equations.

The test case chosen is a two degree of freedom case from [41], which used a NACA64A010 aerofoil. The structural parameters used for the calculations are as follows:

$$a_h = -0.2, x_\alpha = 0.2, r_\alpha = 0.5, \frac{\omega_h}{\omega_\alpha} = 0.3, \mu = 23.48. \quad (12)$$

The response computed is dependent on the values of Mach number and speed index. For a particular Mach number, the structural response to a disturbance can be decaying, neutrally stable, diverging, limit cycle oscillation or explosive flutter. Which form is taken is determined by the magnitude of the speed index, which represents the ratio of the aerodynamic forces to structural stiffness.

The neutrally stable value of speed index for the section can be found by computing the response at several values of speed index for a set Mach number. This was performed for a transonic case (Mach 0.85), using a 147×32 mesh. The phase lag introduced by the weak coupling scheme decreases with decreasing time-step, but decreasing the time-step means increasing the number of time-steps per period and hence the required CPU time. Hence, the accuracy and CPU requirements of the weak and strong coupling schemes have been analysed. The neutrally stable value of speed index for Mach 0.85 was computed using a large number of real time-

steps, 360 per period. The number of real time-steps was then reduced and the effect of weak and strong coupling considered, in terms of rate of decay of heave amplitude. Figure 2 shows the rate of decay and CPU time against real time-step size. Even with only 50 time-steps per cycle the strong coupling scheme shows less than 0.1% error in rate of decay (growth in this case), whereas for a similar error the weak coupling scheme needs 120 time-steps per cycle. However, the CPU plot shows that only for low numbers of real time-steps is the strong coupling scheme more expensive, but in this region the weak coupling is not of acceptable accuracy. As a flight control system is to be integrated which cannot function with inherent phase lag, the strong coupling scheme was chosen.

4.2 Energy Considerations

It is interesting to consider the energy transfer from fluid to structure, and vice versa, during a simulation. The general energy identity, (derivable from Lagrange's equation) is given by

$$E_{total} = KE + PE = E_o + W_{ext} \quad (13)$$

where E_{total} is the total mechanical energy of the structure, consisting of kinetic energy (KE) and potential energy (PE). E_o is the initial energy of the structure, i.e. the energy that the structure has at time=0, and W_{ext} is the work done by external forces such as the aerodynamic forces.

$W_{ext} > 0$ indicates that work is being done by the fluid. If the amplitude of structural oscillation grows then W_{ext} and E_{total} will also grow but following the energy identity given by equation (13), the difference between the total energy and the work done by the aerodynamic forces should be constant.

5 Two Degree of Freedom Response

A two degree of freedom test case due to Isogai [42] was first considered. The aeroelastic parameters used are

$$a_h = -2.0, x_\alpha = 1.8, r_\alpha = 1.87, \frac{\omega_h}{\omega_\alpha} = 1.0, \mu = 60. \quad (14)$$

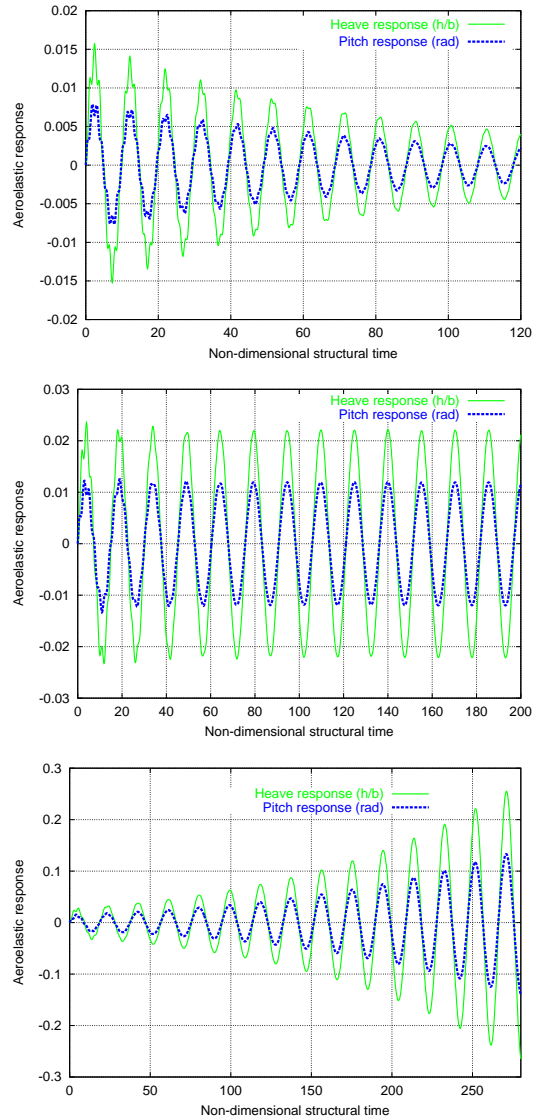


Fig. 3 Aeroelastic response, $U^*=0.30, 0.5025, 0.7$.

This represents a section of a swept back wing, since the elastic axis is ahead of the leading edge.

Aeroelastic responses for heave and pitch for speed index, U^* , values of 0.30, 0.5025 and 0.70 at a Mach number of 0.85 are shown in figure 3. At the lower value of speed index the responses are decayed. As U^* increases the response reaches a neutrally stable condition, and this is termed the flutter point (0.5025 in this case). When the speed index is increased further, the extracted energy overpowers the structural stiffness, hence diverging responses which settle to limit cycle oscillation (LCO) are obtained. Further increase in speed index will cause

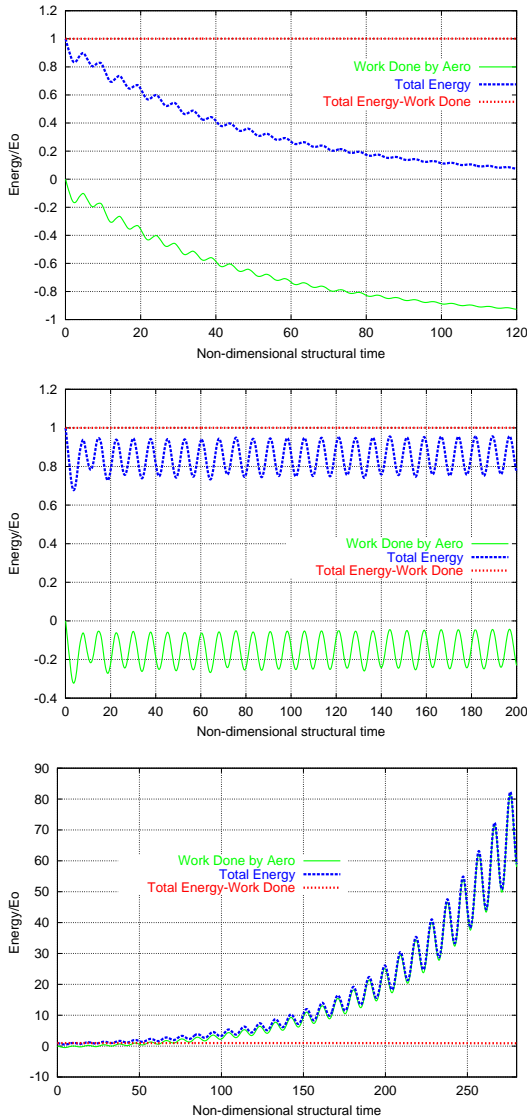


Fig. 4 Energy variations, $U^*=0.30, 0.5025, 0.7$.

explosive flutter that leads to structural failure.

Figure 4 displays the energy variations for the three cases above. The energy is nondimensionalized by the initial energy E_o , so that the difference of the total energy and the work done by external forces should be equal to one as time increases. It can be seen from figure 4 that this difference remains constant and equal to the initial energy E_o , thus proving that the numerical scheme used is energy conserving.

The flutter point is located for a particular Mach number by computing the time-response for several values of speed index, and analysing the rate of decay for each one. When the speed index is found at which the rate of decay is zero,

this is the flutter speed index at that Mach number. If the process of locating the flutter point is repeated for several Mach numbers the flutter boundary of the aerofoil can be computed. The computed flutter boundary is shown in figure 5, which also shows results due to Jameson [5], Isogai [42], and Bendiksen [4]. The results compare well.

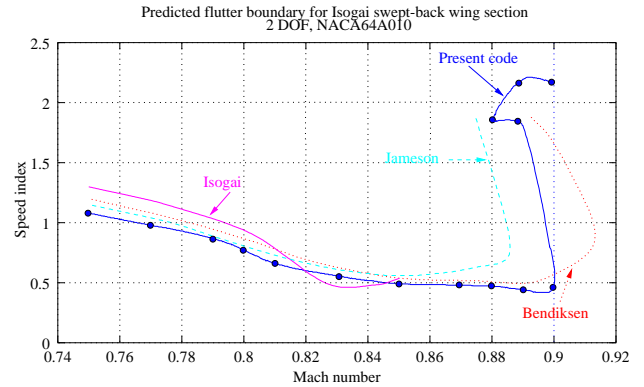


Fig. 5 Isogai model predicted flutter boundary

One interesting point to consider is the phase difference between the heave and pitch motion. Figure 6 shows the phase difference for varying Mach number and speed index. In the lower transonic region the heave and pitch motion are in phase even far above the flutter point. As the Mach number and speed index increase this difference increases almost linearly, until there is a rapid change to antiphase motion at high Mach number.

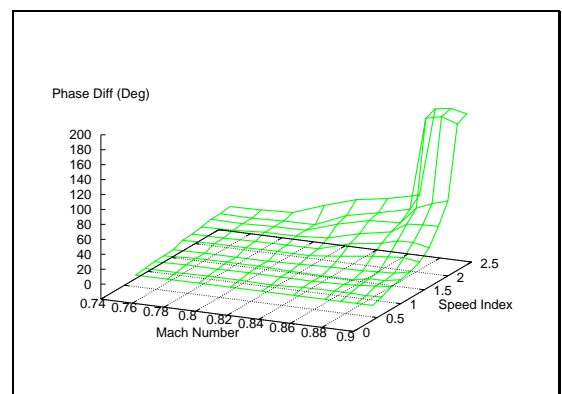


Fig. 6 Phase Difference plot, Isogai Model

5.1 Three Degree of Freedom Response

A third degree of freedom was added to the NACA64A010 case used earlier. The structural parameters used for the calculations are as follows, see [41]:

$$a_h = -0.2, x_\alpha = 0.2, r_\alpha = 0.5, \frac{\omega_h}{\omega_\alpha} = 0.3, \mu = 23.48,$$

$$x_\beta = 0.008, r_\beta = 0.06, \frac{\omega_\beta}{\omega_\alpha} = 1.5, C_\beta = 0.5 \quad (15)$$

The computed flutter boundary of the aerofoil is shown in figure 7. The figure also shows results obtained by DLR [41], and the two flutter boundaries compare very well.

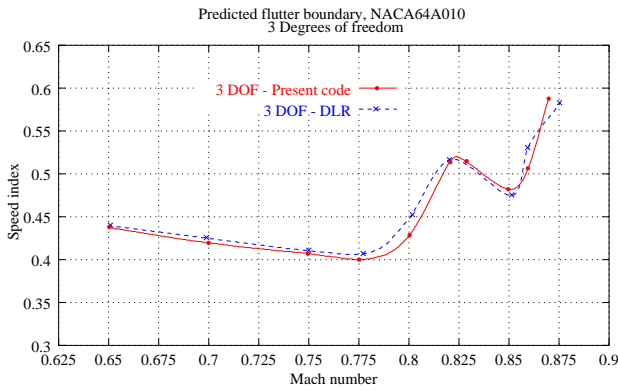


Fig. 7 Predicted flutter boundary for 3 DoF

6 Aeroservoelastic Simulation

Active control has been implemented within the aeroelastic solver, in order to investigate active means of transonic flutter suppression. A simple control law is used which relates the required flap deflection angle, β_c , to the motion of the main aerofoil surface (heave and pitch degrees of freedom). Hence, β_c is evaluated according to the following equation

$$\beta_c = [G_1, G_2] \begin{Bmatrix} \xi \\ \alpha \end{Bmatrix} + [G_3, G_4] \begin{Bmatrix} \dot{\xi} \\ \dot{\alpha} \end{Bmatrix} + [G_5, G_6] \begin{Bmatrix} \ddot{\xi} \\ \ddot{\alpha} \end{Bmatrix} \quad (16)$$

where the G 's are the gains of the system.

The flap is moved according to the demanded deflection angle β_c . However, instead of moving the flap by β_c degrees within a certain amount of time (according to the flap deflection rate), the required angle is converted into equivalent control hinge moment (CHM) which is blended into

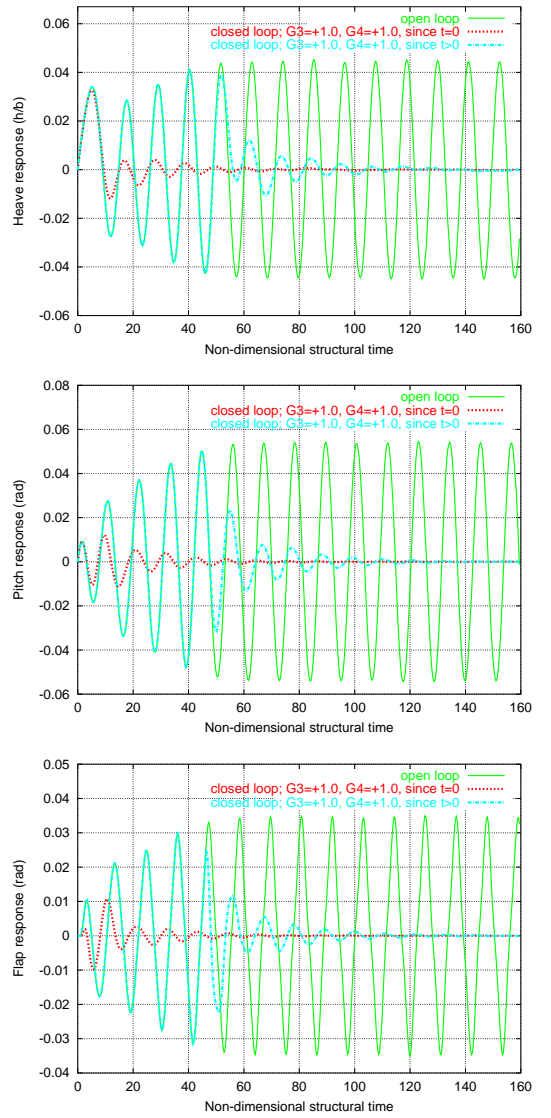


Fig. 8 Positive velocity feedback; $G_3 = +1.0$, $G_4 = +1.0$, $U^* = 1.05 U_f^*$

the open loop aeroelastic equations as the external moment acting on the hinge axis, hence only affecting the β degree of freedom. There are now two hinge moments on the right hand side of the aeroservoelastic equation, the aerodynamic hinge moment (AHM) and the control hinge moment (CHM) as shown by equation 17

$$x_\beta \ddot{\xi} + [(C_\beta - a_h)x_\beta + r_\beta^2] \ddot{\alpha} + r_\beta^2 \ddot{\beta} + \frac{4M_\infty^2 \gamma}{U^{*2} \mu} r_\beta^2 \left(\frac{\omega_\beta}{\omega_\alpha} \right)^2 \beta$$

$$= \underbrace{\frac{8M_\infty^2 \gamma}{\pi \mu} C_H}_{AHM} + \underbrace{\frac{4M_\infty^2 \gamma}{U^{*2} \mu} r_\beta^2 \left(\frac{\omega_\beta}{\omega_\alpha} \right)^2 \beta_c}_{CHM} \quad (17)$$

This is because it is impossible to guarantee that the flap will move from β to $\beta + \beta_c$ within a certain amount of time. By converting the required angle to the equivalent control hinge moment the flap dynamics are accounted for.

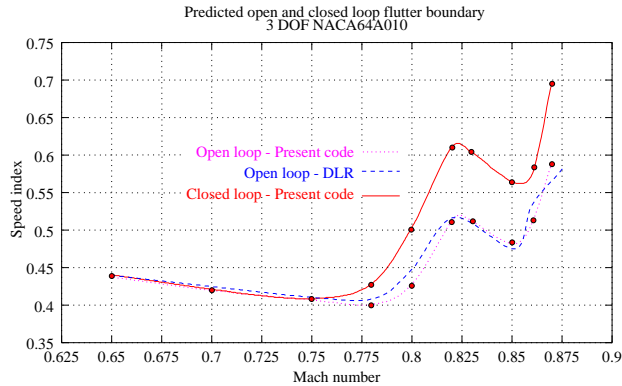


Fig. 9 Control law effectiveness

The same time marching scheme is used to integrate the aeroservoelastic equation of motion, the only change lies in the representation of the right hand side force. It is now given by $\mathbf{f} = \mathbf{f}_a + \mathbf{f}_c$ where \mathbf{f}_c is the control forces and is given by $\mathbf{f}_c = \{0, 0, CHM\}^T$. The work done by external forces now includes an extra term due to the control surface.

6.1 Results

Closed loop simulations were performed using the active control. A Mach number of 0.85 was chosen, and the speed index was 5% above the flutter speed, i.e. corresponding to an unstable response. Different gain combinations were considered to determine the optimum combinations to be used. It was found that G_1 , G_2 , G_5 and G_6 fail to suppress the flutter, whereas G_3 and G_4 successfully suppressed the motion. The most effective combination was to use G_3 and G_4 together. Figure 8 show the heave, pitch and flap responses for $M = 0.85$, and $U^* = 1.05U_{flutter}^*$. The initial disturbance was $\xi = \alpha = 0.01$ and the gains were $G_3 = G_4 = 1.0$. Two situations were considered: implementing the active control immediately, and at some later time. It is clear that the active control has managed to “drain” the structural energy very quickly, even when the distur-

bance has sufficient time to grow.

The flutter boundaries are shown in figure 9. The control law works very effectively within the transonic region, where the shock position can be affected by the flap. An increase of up to 19% in the allowable speed index can be achieved.

The mechanics of transonic flutter and active control were investigated, by considering a more unstable case. Figure 10 shows a series of flowfield Mach contours for $M = 0.85$, and $U^* = 1.10U_{flutter}^*$. The same aerofoil was used, but the grid density was increased to 211×40 to capture the shocks more sharply. Contours are plotted every quarter period, for seven periods, and the active control was switched on at the end of the third cycle. The flap is clearly effective in controlling the shock motion in this case.

7 Conclusions

Numerical simulations of transonic flutter and active control have been presented. Coupling of independent aerodynamic and structural dynamic codes has been analysed and it has been shown that only for large real time-steps is the simpler weak coupling scheme computationally cheaper than strong coupling. However, in this region the weak coupling scheme is not of acceptable accuracy. A simple control system has been integrated with the coupled code, and since this requires perfect synchronisation of fluid, structure and control signal, the strong coupling scheme has been adopted.

The coupled scheme has been used to simulate time responses to structural disturbances for various Mach numbers and speed indices, and flutter boundaries computed for two and three degree of freedom cases. Furthermore, the structural model has been extended to include an actively controlled trailing edge flap, and this has successfully been used to increase the stability margin by means of control surface motion. The aerofoil heave and pitch rate feedback signal was found to give the best suppression results, and for the NACA64A010 aerofoil, an increase of up to 19% in the allowable speed index can be achieved within the transonic region.

References

- [1] MacNeal Schwendler Corporation, "MSC/NASTRAN Aeroelastic Analysis" Seminar Notes Version 68, May 1995
- [2] Bendiksen, O.O., and Kousen, K.A., "Transonic Flutter Analysis Using the Euler Equations" AIAA Paper No. 87-0911-CP, 1987
- [3] Kousen, K.A. and Bendiksen, O.O., "Non-Linear Aspects of the Transonic Aeroelastic Stability Problem" AIAA Paper No. 88-2306. Also in AIAA/ASME/ASCE/AHS 29th Structures, Structural Dynamics and Material Conference, 1988
- [4] Kousen, K.A. and Bendiksen, O.O., "Limit Cycle Phenomena in Computational Transonic Aeroelasticity" Journal of Aircraft, Vol. 31, No. 6, Nov.-Dec. 1994, pp 1257-1263
- [5] Alonso, J.J., and Jameson, A., "Fully-Implicit Time-Marching Aeroelastic Solutions" AIAA Paper No. 94-0056, Jan. 1994
- [6] G.P. Guruswamy, "Unsteady Aerodynamic and Aeroelastic Calculations for Wings Using Euler Equations" AIAA Journal, Vol. 28, No. 3, pp. 461-469, March 1990
- [7] B.A. Robinson, J.T. Batina, H.T.Y. Yang, "Aeroelastic Analysis of Wings Using the Euler Equations with a Deforming Mesh" Journal of Aircraft, Vol. 28, No. 11, pp.781-788, November 1991
- [8] K.J. Badcock, G.Sim, B.E. Richards "Aeroelastic Studies using Transonic Flow CFD Modelling" International Forum on Aeroelasticity and Structural Dynamics 1995, pp 18.1-18.12, June 1995
- [9] Prananta, B.B., Hounjet, M.H.L., and Zwaan, R.J., "Thin Layer Navier-Stokes Solver and its Application for Aeroelastic Analysis of an Airfoil in Transonic Flow" International Forum on Aeroelasticity and Structural Dynamics 1995, June 1995, pp 1.....1-1.9
- [10] Prananta, B.B., Hounjet, M.H.L. "Aeroelastic Simulation with Advanced CFD Methods in 2-D and 3-D Transonic Flow" Symposium Unsteady Aerodynamics, RAeS, London, July 1996.
- [11] J.J. Meijer, M.H.L. Hounjet, B.J.G. Eussen, and B.B. Prananta, "NLR-TU Delf Experience in Unsteady Aerodynamics and Aeroelastic Simulation Applications" AGARD Report No. 822, Numerical Unsteady Aerodynamic and Aeroelastic Simulation, pp. 11-1 - 11-21, March 1998
- [12] D.M. Schuster, P.S. Beran, L.J. Huttshell "Application of the ENS3DAE Euler/Navier-Stokes Aeroelastic Method" AGARD Report No. 822, Numerical Unsteady Aerodynamic and Aeroelastic Simulation, pp. 3-1 - 3-11, March 1998
- [13] H. Försching, "Challenges and Perspectives in Computational Aeroelasticity" International Forum on Aeroelasticity and Structural Dynamics 1995, pp. 1.1-1.9, June 1995
- [14] R.M. Bennett, J.W. Edwards, "An Overview of Recent Development in Computational Aeroelasticity" AIAA 98-2421, 29th AIAA Fluid Dynamics Conference, Albuquerque NM, 1998.
- [15] T.E. Noll, "Aeroservoelasticity" Chapter 3 in Flight-Vehicle Materials, Structures, and Dynamics-Assessment and Future Direction, Vol.5 Structural Dynamics and Aeroelasticity, A.K. Noor and S.L. Venneri, pp.179-212, 1993
- [16] E. Nissim, "Recent Advances in Aerodynamic Energy Concept for Flutter Suppression and Gust Alleviation Using Active Controls" NASA TN D-8519, 1977
- [17] E. Nissim, A. Caspi, I. Lottati "Application of the Aerodynamic Energy Concept to Flutter Suppression and Gust Alleviation by use of Active Controls" NASA TP 1137, 1978
- [18] E. Nissim, and I. Abel, "Development and Application of an Optimization Procedure for Flutter Suppression Using the Aerodynamic Energy Concept" NASA TP 1137, 1978
- [19] E. Nissim, "Design of Control Laws for Flutter Suppression Based on the Aerodynamic Energy Concept and Comparisons With Other Design Methods" NASA TP 3056, 1990
- [20] M. Karpel, "Design for Active Flutter Suppression and Gust Alleviation Using State-Space Aeroelastic Modelling" Journal of Aircraft, Vol. 19, No. 3, pp.221-227, March 1982
- [21] J.T. Batina, T.Y. Yang, "Application of Transonic Codes to Aeroelastic Modelling of Airfoils Including Active Controls" Journal of Aircraft, Vol. 21, No. 8, pp.623-630, August 1984
- [22] G.P. Guruswamy, E.L. Tu, "Transonic Aeroelasticity of Fighter Wings with Active Control Surfaces" AIAA Journal VOL.27, No.6, pp.788-793, 1988
- [23] G.P. Guruswamy "Integrated Approach for Active Coupling of Structures and Fluids" AIAA J Vol.27, No.6, pp788-793, 1988.
- [24] C.G. Pak, P.P. Friedman, E. Livne, "Transonic Adaptive Flutter Suppression Using Approximate Unsteady Time Domain Aerodynamics" AIAA-91-0986-CP
- [25] D. Guillot, P.P. Friedman, "A Fundamental Aeroservoelastic Study Combining Unsteady CFD with Adaptive Control" AIAA 94-1721
- [26] D. Guillot, P.P. Friedman, "Adaptive Control of Aeroelastic Instabilities in Transonic Flow Using CFD Based loads" International Forum on Aeroelasticity and Structural Dynamics 1995, pp 73.1-73.13, June 1995
- [27] E. Nissim, "Flutter Suppression Using Active Controls Based on the Concept of Aerodynamic Energy" NASA TN D-6199, 1971
- [28] Jameson, A., Schmidt, W., Turkel, E., "Numerical Solutions Of the Euler Equations by Finite Volume Methods Using Runge-Kutta Time Stepping Schemes" AIAA-Paper No. 81-1259, 1981.
- [29] Kroll, N., and Jain, R.K., "Solution of Two Dimensional Euler Equations - Experience with a Finite Volume Code" DLR Report, DFVLR-FB 87-41, October 1987.
- [30] Jameson, A., "Time Dependent Calculations Using Multigrid, with Applications to Unsteady Flows Past Airfoils and Wings", AIAA Paper 91-1596.
- [31] Gaitonde, A.L., "A Dual-Time Method for the Solution of the unsteady Euler Equations" The Aeronautical Journal of the Royal Aeronautical Society, Oct. 1994, pp 283-291
- [32] W.J. Gordon, and C.A. Hall, "Construction of Curvilinear Coordinates Systems and Applications to Mesh Generation" International Journal for Numerical Methods in Engineering, Vol.7, pp. 461-477, 1973
- [33] W.J. Gordon, and L.C. Thiel, "Transfinite Mappings and Their Application to Grid Generation" Numerical Grid Generation, edited by J.F. Thompson, North Holland, 1982
- [34] L.E. Eriksson, "Generation of Boundary Conforming Grids Around Wing-Body Configurations Using Transfinite Interpolation" AIAA Journal Vol.20, No.10, pp.1313-1320, October 1982
- [35] Allen, C.B., "Central-Difference and Upwind Biased Schemes for Steady and Unsteady Euler Aerofoil Flows", Aeronautical Journal, Vol. 99, pp52-62, February 1995.
- [36] Allen, C.B., "The Reduction of Numerical Entropy Generated by Unsteady Shockwaves", Aeronautical Journal, Vol. 101, No. 1001, pp9-16, January 1997.
- [37] P.D. Thomas, and C.K. Lombard, "Geometric Conservation Laws and its Application to Flow Computations on Moving Grid" AIAA Journal, Vol.17, No.10, pp.1030-1037, 1979
- [38] Djayapertapa, L. and Allen, C.B., "Time-Marching Analysis of Aeroservoelasticity", Paper 1, RAeS Aerodynamics Conference, London, April 2001.
- [39] Dowell, E.H., Editor, [et.al.], "A Modern Course in Aeroelasticity" - 3rd revision and enlarged edition Kluwer Academic Publishers, Boston 1994
- [40] Bathe, K.J., "Finite Element Procedures in Engineering Analysis" Prentice Hall, Englewood Cliffs, New Jersey, 1982.
- [41] Schulze, S. "Transonic Aeroelastic Simulation of a Flexible Wing Section" AGARD Report No. 822, Numerical Unsteady Aerodynamic and Aeroelastic Simulation, pp. 10-1 - 11-20, March 1998
- [42] Isogai, K., "On the Transonic-Dip Mechanism of Flutter of a Sweptback Wing" AIAA Journal, Vol. 17, No.7, pp. 793-795, July 1979

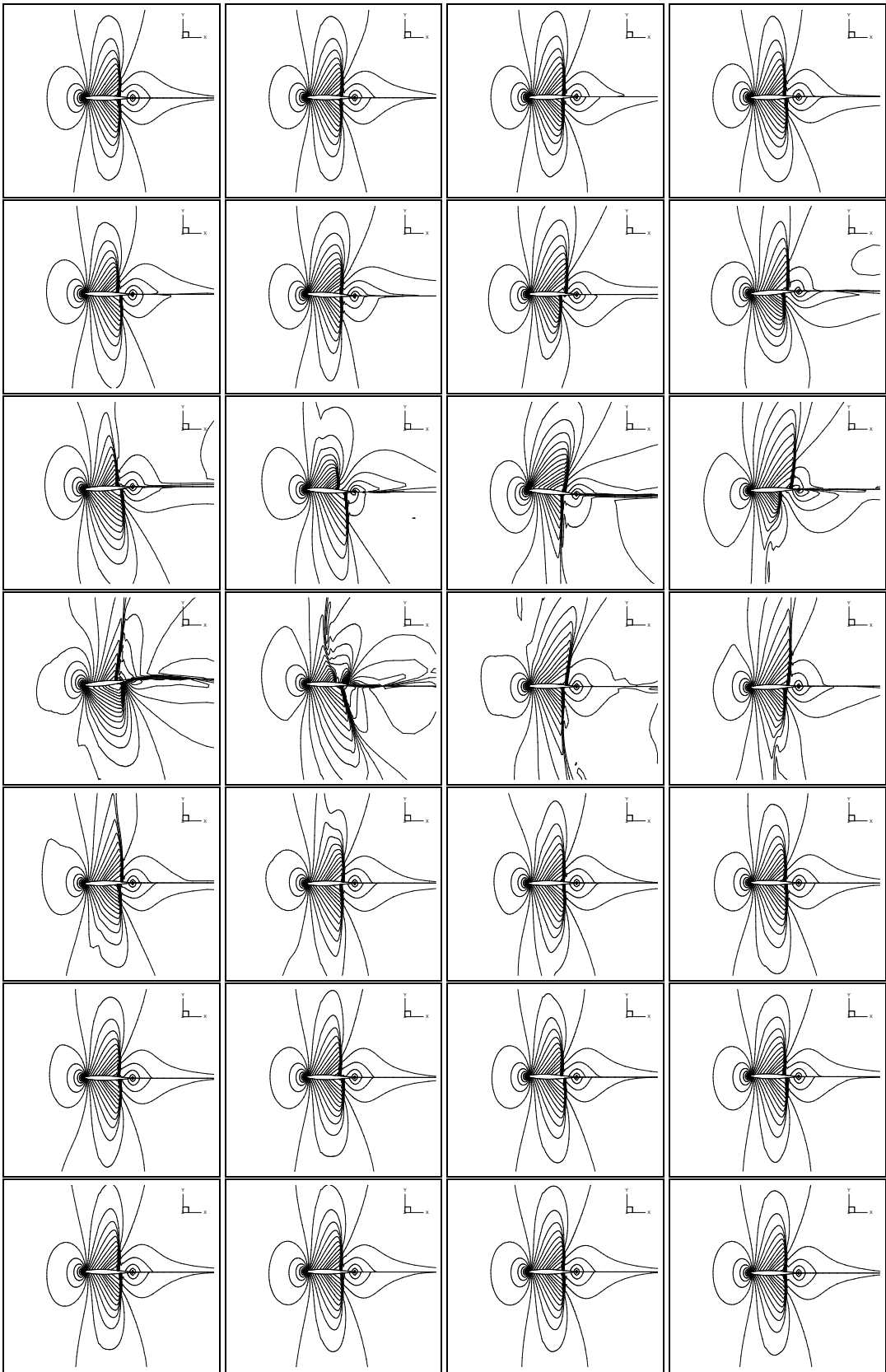


Fig. 10 Closed loop flowfield Mach contours